AIAA JOURNAL
Vol. 40, No. 7, July 2002

Accuracy of Parabolized Navier–Stokes Schemes for Stability Analysis of Hypersonic Axisymmetric Flows

Vahid Esfahanian* and Kazem Hejranfar†
University of Tehran, 11365-4563 Tehran, Iran

The accuracy of the parabolized Navier–Stokes (PNS) and globally iterated PNS (IPNS) schemes for use as basic flows is studied for stability analysis of hypersonic axisymmetric flow over blunt and sharp slender cones at Mach 8. The numerical solution of the PNS and IPNS models is obtained by using the implicit finite difference algorithm of Beam and Warming with a shock-fitting procedure. Both the PNS and IPNS solutions are thoroughly verified and compared with the thin-layer Navier–Stokes (TLNS) solution and experimental data. The stability analysis and transition prediction are performed using the parallel-flow linear stability theory together with the e^N method. A systematic sensitivity study is performed for basic state solutions, including profiles and their derivatives, and spatial growth rates obtained from the PNS and IPNS models. The basic flow and stability results and the predicted transition location based on the PNS model are qualitatively in good agreement with those of other theoretical investigations using various basic flow models. Improved agreement with the TLNS model for both basic state solution and stability results is achieved when the IPNS model is applied. Attention is concentrated on those features of the numerical methods of the basic flow computation that need particular care if adequate stability results are to be obtained. The study shows that the number of grid points, the grid distribution, and the amount of numerical dissipation have significant effects on the stability results. Moreover, indications are that careful numerical solutions of the PNS and IPNS schemes as laminar basic flow calculations lead to a more practical transition prediction tool in hypersonic flows.

Nomenclature

D	=	differential operator, identical to $\mathrm{d}/\mathrm{d}y_n$
$\boldsymbol{D}_e, \boldsymbol{D}_i$	=	explicit and implicit dissipation terms
E	=	total energy per unit volume
$\boldsymbol{F}, \boldsymbol{G}, \boldsymbol{H}$	=	transformed flux vectors
f	=	frequency
G	=	generalized inflection profile, $\mathrm{d}/\mathrm{d}y_n(\rho\,\mathrm{d}U/\mathrm{d}y_n) - \kappa_2\rho\,\mathrm{d}U/\mathrm{d}y_n$
h_1, h_2, h_3	=	scale factors in ξ, η, and ϕ directions
J	=	Jacobian, $\xi_x\eta_y - \xi_y\eta_x$
L	=	reference length, R_N for blunt cone and $S^*_{\max}$ for sharp cone
l_e	=	Blasius length based on boundary-layer edge conditions, $\sqrt{(\nu_e^* S^*/U_e^*)}$
l_∞	=	Blasius length based on freestream conditions, $\sqrt{(\nu_\infty^* S^*/U_\infty^*)}$
M	=	Mach number
N	=	N factor
p	=	pressure
$\boldsymbol{Q}$	=	flowfield vector, $(U, V, W, p, T)^T$
$Re_{e,l}$	=	Reynolds number based on boundary-layer edge conditions and l_e, $U_e^* l_e/\nu_e^* = \sqrt{(U_e^* S^*/\nu_e^*)}$
$Re_{e,S}$	=	Reynolds number based on boundary-layer edge conditions and S^*, $U_e^* S^*/\nu_e^*$
Re_∞	=	Reynolds number based on freestream conditions and L, $U_\infty^* L/\nu_\infty^*$
$Re_{\infty,l}$	=	Reynolds number based on freestream conditions and l_∞, $U_\infty^* l_\infty/\nu_\infty^* = \sqrt{(U_\infty^* S^*/\nu_\infty^*)}$
R_N	=	dimensional nose radius
r	=	body radius
S	=	arc length along the body
T	=	temperature
t	=	time
U, V, W	=	velocity components in ξ, η, and ϕ directions
$\boldsymbol{U}$	=	solution vector, $J^{-1}(\rho, \rho u, \rho v, E)^T$
U_c	=	contravariant velocity in ξ direction, $\xi_x u + \xi_y v$
u, v	=	velocity components in x and y directions
x, y	=	Cartesian coordinates
α, β	=	wave numbers in ξ and ϕ directions
$-\alpha_i$	=	spatial growth rate
$\bar{\beta}$	=	clustering parameter
γ	=	ratio of specific heats
Δ, ∇	=	forward and backward difference operators
ϵ_e, ϵ_i	=	explicit and implicit dissipation coefficients
θ_c	=	cone half-angle
κ_2	=	curvature term, $(\partial h_3/\partial y_n)/h_3 = \cos\theta_c/h_3$
ν	=	kinematic viscosity
ξ, η	=	computational coordinates
ξ, η, ϕ	=	intrinsic curvilinear coordinates
ρ	=	density
Ω_p	=	pressure underrelaxation coefficient
ω	=	circular frequency
$\bar{\omega}$	=	weighting function

Subscripts

b	=	basic flow
e	=	boundary-layer edge condition
i	=	inviscid vector or imaginary part
k	=	old time level
m	=	intermediate time level
n	=	normal to the wall
r	=	real part
s	=	shock condition
v	=	viscous vector
w	=	wall condition
∞	=	freestream condition

Superscripts

i	=	marching index
$*$	=	dimensional quantity

Received 13 March 2001; revision received 11 December 2001; accepted for publication 11 December 2001.

*Associate Professor, Mechanical Engineering Department, North Amir-Abad Avenue.

†Ph.D. Candidate, Mechanical Engineering Department, North Amir-Abad Avenue.

$'$ = disturbance quantity
$\hat{}$ = amplitude quantity

Introduction

THE accurate determination of viscous hypersonic flowfields past long, slender axisymmetric blunt bodies is of prime interest to the aerodynamic designer of high-speed vehicles both from an aerodynamic and a heat transfer standpoint. Additionally, for such vehicles, the knowledge of the transition Reynolds number and the use of suitable turbulence modeling are key factors in accurately predicting the skin-friction drag and aerodynamic heating. Therefore, the prediction of the transition location is of great importance for hypersonic vehicles because the drag and the heating rate are strongly dependent on the location where transition occurs.

Hypersonic transition experiments of blunted-cone forebodies by Stetson[1] and Stetson et al.[2] indicate that a small nosetip bluntness makes significant changes in the local transition Reynolds number along the frustum. It is found that, by adding a blunt nose to a sharp cone, transition is delayed to a distance farther downstream of the nosetip. On the other hand, for a large nosetip bluntness, transition may occur prematurely on the nose itself, and hence, the transition Reynolds number is greatly reduced. This rearward movement of the transition location is known as "transition reversal phenomena." Therefore, the transition Reynolds number is very sensitive to the bluntness ratio of the body, and any attempt toward understanding the process of transition of blunt bodies will have a significant role in the design of high-speed vehicles.

Most theoretical stability studies of hypersonic axisymmetric flows over blunt bodies known in the literature are based on the parallel-flow linear stability analysis.[3–7] The hydrodynamic stability theory is useful in indicating the major dominant effects that hasten or delay transition in a relative sense. In addition, the transition location can be approximately predicted using a semi-empirical correlation such as the e^N method.

The stability analysis of the flow over blunt slender bodies at high Mach numbers faces three major problems[4,5]: 1) the computation of the basic flowfield and the derivatives of the flow variables with sufficient accuracy, 2) the formulation of the stability problem with proper account for the flow physics, and 3) the accurate solution of the stability equations. Two models for an accurate computation of the basic flow over blunt axisymmetric bodies are the thin-layer Navier–Stokes (TLNS) equations and the Euler/second-order boundary-layer (EUBL) equations.

The TLNS model has been used by Esfahanian[4] and Herbert and Esfahanian[5] as a basic flow to study the stability analysis of hypersonic flow over a blunt cone at Mach 8 for the conditions of the experiment of Stetson et al.[2] [the Stetson–Thompson–Donaldson–Siler (STDS) blunt-cone case]. The numerical solution of the TLNS model was obtained by the Beam–Warming method[8] using a shock-fitting procedure. Esfahanian[4] and Herbert and Esfahanian[5] devoted considerable effort to obtain an accurate solution of the TLNS model by employing the smallest possible numerical dissipation value. They emphasized the need for a correct calculation of the basic flow variables and also their derivatives as a prerequisite for stability computations. Although they used an accurate basic flow by employing the TLNS model, the associated stability results showed much larger maxima for the second-mode spatial growth rate than that of the experiment.

Kufner et al.[6] performed a detailed basic flow sensitivity study to explain the discrepancies between experimental and previously obtained theoretical spatial growth rates for the STDS blunt-cone case. They used the TLNS equations as a basic flow, which was numerically solved using a shock-capturing upwind scheme with total variation diminishing properties. According to their studies, the effects of cooling and heating, as well as wall temperature reductions or boundary-layer thickness variations, cannot be used to explain the discrepancies. They have claimed that the discrepancies between theoretical and experimental results seem to be caused by experimental problems. In addition, the stability results of Kufner et al.,[6] namely, the spatial growth rates, disagreed with those obtained by the TLNS model[4,5] solved by the Beam–Warming method, and the maximum value was lower.

Because the numerical computations of hypersonic viscous flows using the TLNS equations are time consuming and require very high storage and computer speed, Stilla[7] used an Euler/boundary-layer scheme in combination with a second-order boundary-layer theory to compute the basic flow for investigating the stability analysis of the STDS blunt-cone case. Results of his sensitivity study showed the importance of viscous–inviscid interaction and entropy-layer resolution. Although the computation of the basic flow and the stability results based on the EUBL model agree very well with the TLNS computation based on the Beam–Warming scheme, providing the inviscid solution and the edge boundary conditions (including the displacement effect) and matching the inviscid and viscous regions are cumbersome.

Consequently, for practical engineering prediction of transition location, one has to choose a more efficient way of computing the basic flow. An appropriate candidate for the basic flow computation is the parabolized Navier–Stokes (PNS) equations. The PNS equations are paraboliclike with respect to the streamwise direction. Hence, similar to the boundary-layer equations, the PNS equations are solved by marching an initial data plane in space rather than by marching the entire flowfield in time, as is done for the TLNS equations. Thus, the computational effort and required storage can be significantly reduced using the PNS equations. Unlike the boundary-layer equations, however, the PNS equations are valid in both the viscous and inviscid portions of the flowfield. Therefore, the PNS equations are suitable for solving the regions of the flowfield, such as the entropy layer, in which a strong interaction exists between these regions (Fig. 1).

The effect of nose bluntness on boundary-layer stability and transition for the conditions of Stetson et al.[2] has been studied by Malik et al.[3] They computed the basic flow by employing the PNS code that was based on a shock-capturing upwind algorithm. They found that the predicted transition Reynolds number increases due to small nose bluntness as observed by Stetson et al.[2] The stability results obtained by Malik et al.[3] disagree with those obtained by the TLNS model[4,5] solved by the Beam–Warming method and the EUBL model,[7] but their results[3] are closer to the STDS blunt-cone experiment. Malik et al.[3] observed wiggles in the pressure profiles. However, they did not investigate the accuracy of basic flow variables and their derivatives in comparison with Navier–Stokes solutions and their effects on the stability results.

To clarify some of the open questions, considerable efforts have been devoted to develop accurate PNS and iterated PNS (IPNS) codes[9,10] compatible with the TLNS code developed by Esfahanian[4] and Esfahanian et al.[11] The study of the STDS blunt-cone case has shown that the results of the present PNS code are relatively accurate for the basic flow variables, but due to the omitting of the elliptic contribution of the streamwise pressure gradient, small deviations exist in the subsonic region of the derivatives of flow variables, which may affect the accuracy of the stability results.[12] Therefore, the globally IPNS model, which is computationally more efficient than the TLNS model, is used to account for the full pressure gradient in the subsonic viscous region to improve the accuracy of basic state variables and their derivatives, as well as stability results.[13]

In the present work, the accuracy of the PNS and IPNS models for use as basic flows is investigated for the stability analysis of hypersonic axisymmetric flow over the blunt and sharp slender cones

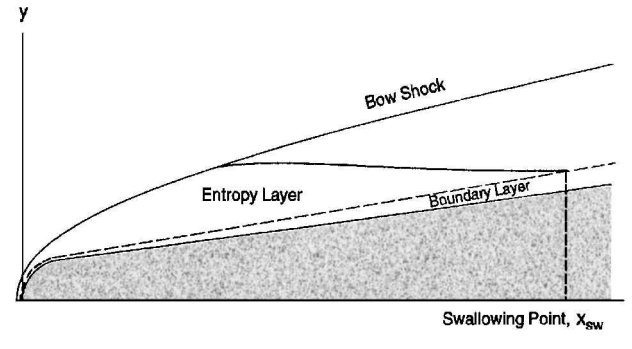

Fig. 1 Physical model for hypersonic flow past a blunt cone.

(the STDS cases) at Mach 8. A sensitivity study of basic state profiles, their derivatives, and stability results is performed. The effect of number of grid points, grid distribution, and amount of numerical dissipation used in the PNS equations is also investigated. The present computations for both sharp and blunt cones are compared with available theoretical and experimental results, and some of the observed discrepancies among theoretical studies are also discussed.

Benchmark Cases

The geometry and the freestream conditions are adapted to the wind-tunnel cone experiments of Stetson et al.[2,14] Here, both sharp and blunt cones are considered. For the STDS blunt-cone case, the flow conditions are a freestream Mach number of $M_\infty = 8$, a freestream unit Reynolds number of $Re_\infty/m = 8.2021 \times 10^6$, and a freestream temperature of $T^*_\infty = 54.3$ K. For the STDS sharp-cone case, the freestream Mach number is set to $M_\infty = 8$, the freestream unit Reynolds number to $Re_\infty/m = 3.2808 \times 10^6$, and the freestream temperature to $T^*_\infty = 52.75$ K. Both sharp and blunt cones have a half-angle of $\theta_c = 7$ deg, and the study is performed at zero angle of attack. The blunt cone has a spherical nose radius of $R_N = 3.81$ mm, and the freestream Reynolds number based on this length is $Re_\infty = 3.1250 \times 10^4$. The maximum arc length along the body of the sharp cone is set to be $S^*_{\max} = 1.9888$ m, which corresponds to the freestream Reynolds number of $Re_\infty = 6.525 \times 10^6$.

Basic Flow Computations

To carry out the stability analysis and transition prediction, the basic flow needs to be computed with sufficient accuracy. The TLNS model is used for computing the basic flow and for verifying the PNS and IPNS solutions. The TLNS equations are obtained from the full Navier–Stokes equations by neglecting viscous terms associated with the streamwise derivatives. The implicit factored finite difference scheme of Beam and Warming[8] is chosen to solve the TLNS equations. In addition, a shock-fitting procedure is used to obtain an accurate solution in the vicinity of the shock wave. The detailed derivations of the TLNS equations and the numerical algorithm are given in Refs. 4 and 15. The advantage of the Beam–Warming method[8] over upwind schemes is that the numerical dissipation values are fully controllable by the user. Consequently, using the Beam–Warming scheme allows one to study the effect of numerical dissipation on the stability results. In view of the preceding remarks, the Beam–Warming method with the shock-fitting procedure is also applied to the PNS and IPNS models described in the following.

Basic Flow: PNS Model

The PNS equations are obtained by dropping the unsteady term in the TLNS equations and modifying the streamwise pressure gradient in the streamwise momentum equation to permit stable marching. The PNS equations for axisymmetric compressible flow can be written in dimensionless and conservative form in the generalized coordinate system (ξ, η) as follows:

$$\frac{\partial \boldsymbol{F}}{\partial \xi} + \frac{\partial \boldsymbol{G}}{\partial \eta} + \boldsymbol{H} = 0 \tag{1}$$

where

$$\boldsymbol{F} = \boldsymbol{F}_i, \qquad \boldsymbol{G} = \boldsymbol{G}_i - \boldsymbol{G}_v, \qquad \boldsymbol{H} = \boldsymbol{H}_i - \boldsymbol{H}_v$$

The PNS equations are a mixed set of hyperbolic–parabolic equations in the marching direction, provided that the inviscid flow is supersonic, the streamwise velocity component is everywhere positive, and the streamwise pressure gradient is either dropped or the departure behavior is suppressed using a suitable technique. The presence of the streamwise pressure gradient term in the streamwise convective flux vector permits the upstream influences to occur in the subsonic region of the boundary layer, which leads to exponentially growing solutions referred to as departure solutions.[16] Stable marching of numerical solution of the PNS equations is achieved in the subsonic region of the boundary layer by using the methods proposed by Vigneron et al.[17] and Schiff and Steger.[18] Both methods are implemented in the present PNS code. For this study, the Vigneron et al.[17] technique is used.

In the Vigneron et al.[17] approximation, the streamwise pressure gradient in the momentum equations is split into an implicit contribution and an explicit contribution:

$$\frac{\partial p}{\partial \xi} = \left[\bar{\omega}\frac{\partial p}{\partial \xi}\right]_{\text{implicit}} + \left[(1-\bar{\omega})\frac{\partial p}{\partial \xi}\right]_{\text{explicit}} \tag{2}$$

The weighting function $\bar{\omega}$ is determined as

$$\bar{\omega} = \min\left[1, \frac{\sigma\gamma M_\xi^2}{1 + (\gamma - 1)M_\xi^2}\right] \tag{3}$$

where M_ξ is the local streamwise Mach number and σ is a safety factor to account for nonlinearities in the analysis. To introduce the Vigneron et al.[17] technique into the PNS equations, a new vector $\boldsymbol{F}^*$ is defined as

$$\boldsymbol{F}^* = \boldsymbol{F} - \boldsymbol{P} \tag{4}$$

Thus, the new form of the PNS equations appears as

$$\frac{\partial \boldsymbol{F}^*}{\partial \xi} + \frac{\partial \boldsymbol{P}}{\partial \xi} + \frac{\partial \boldsymbol{G}}{\partial \eta} + \boldsymbol{H} = 0 \tag{5}$$

where the inviscid vectors $\boldsymbol{F}^*$ and $\boldsymbol{P}$ are

$$\boldsymbol{F}^* = J^{-1}\begin{pmatrix} \rho U_c \\ \rho u U_c + \bar{\omega}\xi_x p \\ \rho v U_c + \bar{\omega}\xi_y p \\ (E+p)U_c \end{pmatrix}, \qquad \boldsymbol{P} = J^{-1}\begin{pmatrix} 0 \\ \xi_x(1-\bar{\omega})p \\ \xi_y(1-\bar{\omega})p \\ 0 \end{pmatrix} \tag{6}$$

In this study, the ratio of specific heats is assumed constant, $\gamma = 1.4$, the molecular viscosity μ is determined by the Sutherland law, and the coefficient of thermal conductivity is calculated by assuming a constant Prandtl number, $Pr = 0.72$. Finally, the system of PNS equations is closed by employing the perfect-gas equations of state. The equations are nondimensionalized using the reference lenght L (R_N or $S^*_{\max}$) and freestream conditions.

In the present PNS code, the elliptic part of streamwise pressure gradient term $(\partial \boldsymbol{P}/\partial \xi)$ responsible for upstream disturbance propagation is omitted to permit the space-marching procedure to be stable.

Basic Flow: IPNS Model

To solve the flowfields with significant upstream influences, the omitting of the explicit part of the streamwise pressure gradient may affect the accuracy of basic flow variables and their derivatives. In these cases, the globally IPNS equations, called the reduced Navier–Stokes equations, can be used, and the upstream influences are taken into account by the forward differencing of the elliptic part of streamwise pressure gradient.

The globally IPNS scheme has been used by several investigators, including Rubin,[19] Rakich,[20] Barnett and Davis,[21] and others. The IPNS model presented herein is based on the method proposed by Barnett and Davis. This IPNS scheme utilizes an alternating direction explicit (ADE) procedure which is in the form of a two-step calculation procedure for each global iteration. In the ADE method, the streamwise pressure gradient is split using the Vigneron et al.[17] technique, and a fictitious unsteady term is appended to the elliptic part as follows:

$$\frac{\partial p}{\partial \xi} = \bar{\omega}\frac{\partial p}{\partial \xi} + (1-\bar{\omega})\left[\frac{\partial p}{\partial \xi} - \frac{\partial p}{\partial t}\right] \tag{7}$$

to permit the upstream propagation of information through the subsonic region in a hyperbolic manner.

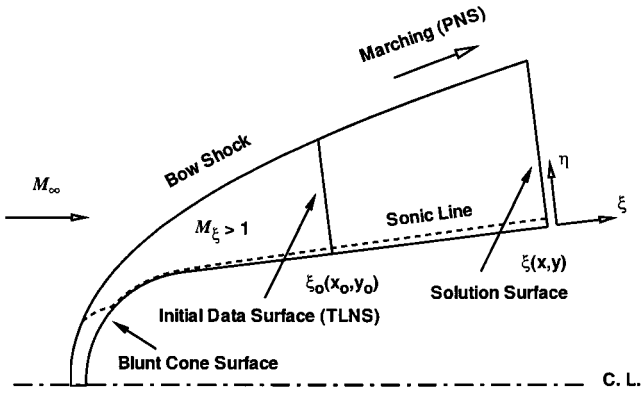

Fig. 2 Marching procedure and initial data surface for starting the PNS solution.

Boundary Conditions and Initial Data

The boundary conditions at the wall consist of no-slip conditions for velocity components, a specified wall-temperature or an adiabatic wall, and zero pressure gradient approximation normal to the wall. The wall for the cases studied here is assumed to be adiabatic. At the upper boundary, the bow shock is fitted using a shock-fitting technique to obtain an accurate solution of the PNS equations near the shock.

The starting data of the PNS equations are provided by the solution of the TLNS equations for the blunt-cone case. Figure 2 shows the initial condition and the marching procedure for the PNS equations. The starting solution on an initial data surface where the inviscid flow is supersonic is obtained from the solution of the TLNS model. The PNS equations are self-starting for the sharp cone case, and the initial data for the space-marching procedure are provided by the conical solution of the PNS equations.

Computational Grid

An algebraic grid scheme is used to compute the basic flowfield. The lines of constant ξ are distributed nearly uniformly along the body surface and are orthogonal to the body. (Some adjustment of the ξ lines was necessary to match the stations used in the STDS experiment.) Orthogonality is required because the solution will be used for the stability analysis. To ensure that the viscous regions are adequately resolved, the lines of constant η are clustered near the body surface according to[16]

$$(x - x_w)/(x_s - x_w) = \bar{a}, \qquad (y - y_w)/(y_s - y_w) = \bar{a} \tag{8}$$

where

$$\bar{a} = 1 + \bar{\beta}\left[\frac{1 - \tilde{a}^{(1-\eta/\eta_{\max})}}{1 + \tilde{a}^{(1-\eta/\eta_{\max})}}\right], \qquad \tilde{a} = \frac{\bar{\beta}+1}{\bar{\beta}-1}$$

in which the clustering parameter $\bar{\beta}$ is typically assigned in the range of 1.001–1.01. The grid is used for all of the TLNS, PNS, and IPNS models.

Numerical Solution

The PNS equations in the generalized coordinate system (5) are solved by the use of the efficient implicit finite difference factored algorithm of Beam and Warming[8] for a spatial-marching scheme. The algorithm for a marching step $\Delta\xi$ can be written in delta form as

$$\left[\left[\frac{\partial \boldsymbol{F}^*}{\partial \boldsymbol{U}}\right]^i + \frac{\theta_1 \Delta\xi}{1+\theta_2}\left[\frac{\partial}{\partial\eta}\left[\frac{\partial \boldsymbol{G}}{\partial \boldsymbol{U}}\right]^i + \left[\frac{\partial \boldsymbol{H}}{\partial \boldsymbol{U}}\right]^i\right]\right]\Delta \boldsymbol{U}^i$$

$$= -\frac{\Delta\xi}{1+\theta_2}\left[\frac{\partial \boldsymbol{G}}{\partial\eta} + \boldsymbol{H}\right]^i + \frac{\theta_2}{1+\theta_2}\Delta \boldsymbol{F}^{i-1} - \Delta \boldsymbol{P}^i$$

$$- \Delta\xi\left[\frac{\partial \boldsymbol{F}^*}{\partial\xi}\right]^i_U - \frac{\theta_1(\Delta\xi)^2}{1+\theta_2}\left[\frac{\partial}{\partial\eta}\left[\frac{\partial \boldsymbol{G}}{\partial\xi}\right]^i_{U,U_\eta} + \left[\frac{\partial \boldsymbol{H}}{\partial\xi}\right]^i_{U,U_\eta}\right] \tag{9}$$

where the derivative $[\partial/\partial \boldsymbol{U}]$ is referred to as Jacobian matrix and the subscripts $\boldsymbol{U}$ and $\boldsymbol{U}_\eta$ represent terms that are evaluated with $\boldsymbol{U}$ and $\boldsymbol{U}_\eta$ held fixed. The algorithm utilizes the first-order backward Euler implicit scheme ($\theta_1 = 1$, $\theta_2 = 0$) in the marching direction ξ and the second-order central scheme in the normal direction η.

The preceding system of equations along with the boundary conditions at the wall and the shock gives a block tridiagonal system of equations for $\Delta \boldsymbol{U}^i$ with a block size of 4×4. A block-tridiagonal solver is used to calculate the incremental solution vector $\Delta \boldsymbol{U}^i$, and then the solution vector is determined as follows:

$$\boldsymbol{U}^{i+1} = \boldsymbol{U}^i + \Delta \boldsymbol{U}^i \tag{10}$$

At each station, the shock slope is iteratively corrected in an explicit manner. The iterative process is repeated at the shock until the solution converges, and then the solution marches on the next solution plane.

High-order dissipation terms must be added to this scheme in order to damp high-frequency oscillations associated with the central differencing of derivatives in the η direction. Therefore, second-order implicit and fourth-order explicit dissipation terms of the form

$$\boldsymbol{D}_i = -\epsilon_i J^{-1}(\nabla_\eta \Delta_\eta) J\left[\frac{\partial \boldsymbol{F}^*}{\partial \boldsymbol{U}}\right]^i \Delta \boldsymbol{U}^i, \qquad \epsilon_i = 2\epsilon_e \tag{11}$$

$$\boldsymbol{D}_e = -\epsilon_e\left[\frac{\partial \boldsymbol{F}^*}{\partial \boldsymbol{U}}\right]^i J^{-1}(\nabla_\eta \Delta_\eta)^2 J \boldsymbol{U}^i, \qquad \epsilon_e < \frac{1}{8} \tag{12}$$

are added to the left- and right-hand sides of Eq. (9). Note that only the explicit dissipation term, $\epsilon_e = 0.01$, is used in the PNS equations. The implicit dissipation term is set to zero, $\epsilon_i = 0$, to obtain a more accurate solution.

Recall that, to solve the single sweep PNS model, the explicit streamwise pressure gradient term ($\Delta \boldsymbol{P}^i$) in Eq. (9) is dropped. For the solution of the IPNS model, the preceding algorithm can be used, and the streamwise pressure gradient term is treated by employing the ADE procedure. The ADE scheme, using a first-order forward difference formula for the explicit pressure gradient term in Eq. (7), is written in two steps as follows[21]:

The first step is

$$\left.\frac{\partial p}{\partial \xi}\right|^{i+1} = \bar{\omega}\frac{p_m^{i+1} - p_m^i}{\Delta\xi} + (1-\bar{\omega})\left[\frac{p_k^{i+2} - p_k^{i+1}}{\Delta\xi} - \frac{p_m^{i+1} - p_k^{i+1}}{\Delta t}\right] \tag{13}$$

In this step, the PNS equations are solved with the streamwise pressure gradient given by Eq. (13). The solution is marched from the upstream to the downstream boundary to obtain the pressure distribution at the intermediate time level p_m.

The second step is

$$\frac{p_k^{i+2} - p_k^{i+1}}{\Delta\xi} - \frac{p_m^{i+1} - p_k^{i+1}}{\Delta t} = \frac{p_{k+1}^{i+2} - p_{k+1}^{i+1}}{\Delta\xi} - \frac{p_{k+1}^{i+1} - p_m^{i+1}}{\Delta t} \tag{14}$$

Equation (14) is solved by marching the solution from the downstream to the upstream boundary to obtain the pressure at the new time level p_{k+1}. This simple relation enforces the propagation of information upstream in a relatively rapid manner.

An appropriate outflow boundary condition for the IPNS solution is provided by setting the streamwise pressure gradient equal to zero at the outer boundary. The IPNS solution requires the initial pressure distribution in the subsonic region. The initial guess can be adequately provided by solving the standard single-sweep PNS model. When this initial condition is provided, the solution of the IPNS model is obtained by the ADE procedure, and the pressure is stored at all stations only in the subsonic region. Then, the process is repeated until the solution converges to a specified convergence criterion.

To accelerate the convergence rate of the IPNS model, the underrelaxation procedure for pressure calculation in the subsonic region is applied as follows:

$$p_{k+1} = \Omega_p p_{k+1} + (1 - \Omega_p) p_k, \qquad \Omega_p \le 1 \tag{15}$$

Step-Size Requirement

Cline and Carey[22] showed that the coupling of the implicit algorithm to an explicit shock-fitting technique for advancing the bow shock introduces an explicit stability restriction on the maximum allowable marching step size at the shock boundary ($\Delta\xi < \Delta\xi_{\max}$). As the solution is marched downstream, the maximum allowable step size increases. In this study, the step size is kept constant in the stability band to prevent decreasing the solution accuracy. The step sizes employed in the downstream marching procedure are $\Delta\xi = 2 \times 10^{-4}$ and 0.1 for the STDS sharp and blunt cones, respectively.

Codes Verification

The TLNS code has been thoroughly verified by comparison with Navier–Stokes solutions and thin-layer solutions of previous investigators. These verifications include the sensitivity of the solution to the number of grid points, the choice of the clustering parameter at fixed Courant–Friedrichs–Lewy number, and the explicit numerical dissipation, which was usually set equal to the time step. Details of these investigations have been reported in Refs. 4 and 11.

The present PNS code has been fully verified and compared with the TLNS code and the experimental results for the STDS blunt-cone case. Considerable efforts have been focused on the PNS code to use the least possible numerical dissipation value. The present IPNS code has been verified using a 10-deg compression ramp, a parabolic bump on a flat plate, and a geometry with multiple embedded regions. The results of the present IPNS code have been compared with other IPNS models and full Navier–Stokes results, which show good agreement. Details of these comparisons have been presented in Refs. 9 and 10.

Linear Stability Analysis

Linear Stability Equations

For stability analysis and transition prediction of hypersonic flow over axisymmetric bodies, the parallel-flow linear stability analysis is employed.[4] The stability calculations of the flow over axisymmetric bodies require the derivation of the disturbance equations in curvilinear coordinates. The disturbance equations are derived from the tensor-analytical form of the Navier–Stokes equations using the body intrinsic curvilinear coordinate system. For the cone frustum, the curvature of the body is zero, and the radius of the body changes linearly with x. Therefore, the scale factors in this orthogonal curvilinear coordinate system (ξ, η, ϕ) are

$$h_1 = 1, \qquad h_2 = 1, \qquad h_3 = r(\xi) + \eta \cos\theta_c \tag{16}$$

The linear stability equations are obtained in the traditional way, that is, the basic flow is perturbed by fluctuations in the flow; therefore, the flowfield vector $\boldsymbol{Q}$ can be decomposed into a steady laminar axisymmetric mean value (basic flow) $\boldsymbol{Q}_b = (U_b, V_b, 0, p_b, T_b)^T$ and an unsteady three-dimensional perturbation quantity $\boldsymbol{Q}' = (U', V', W', p', T')^T$ as follows:

$$\boldsymbol{Q}(\xi, \eta, \phi, t) = \boldsymbol{Q}_b(\xi, \eta) + \boldsymbol{Q}'(\xi, \eta, \phi, t) \tag{17}$$

Then, by substituting these equations into the Navier–Stokes equations and subtracting from the governing equations corresponding to the steady basic flow, one can obtain the governing equations for the disturbances $\boldsymbol{Q}'$. All terms including those arising from longitudinal and transverse curvatures are considered. The streamwise variation of the basic flow is neglected under parallel flow assumption, that is,

$$U_b = U_b(\eta), \qquad V_b = 0, \qquad T_b = T_b(\eta)$$
$$p_b = p_b(\eta), \qquad \rho_b = \rho_b(\eta) \tag{18}$$

Because the disturbances are assumed small, the disturbance equations can be linearized, that is, the terms quadratic or higher in the disturbances and their derivatives may be neglected. When it is assumed that the disturbance vector $\boldsymbol{Q}'$ for an instability wave can be expressed as

$$\boldsymbol{Q}'(\xi, \eta, \phi, t) = \hat{\boldsymbol{Q}}(\eta) \exp[i(\alpha\xi + \beta\phi - \omega t)] \tag{19}$$

the linearized disturbance equations are reduced to the following system of ordinary differential equations:

$$\left(\boldsymbol{A}\frac{\mathrm{d}^2}{\mathrm{d}\eta^2} + \boldsymbol{B}\frac{\mathrm{d}}{\mathrm{d}\eta} + \boldsymbol{C}\right)\hat{\boldsymbol{Q}} = 0 \tag{20}$$

where $\hat{\boldsymbol{Q}} = (\hat{U}, \hat{V}, \hat{W}, \hat{p}, \hat{T})^T$ and $\boldsymbol{A}$, $\boldsymbol{B}$, and $\boldsymbol{C}$ are 5×5 matrices. These linearized equations with the homogeneous boundary conditions constitute an eigenvalue problem as follows:

$$\alpha = \alpha(\omega, \beta) \tag{21}$$

which can be solved by standard eigenvalue techniques. All quantities are scaled with freestream conditions and the length l_∞. Therefore, the nondimensional forms of the wave numbers and the frequency appear as

$$\alpha = \alpha^* l_\infty, \qquad \beta = \beta^* l_\infty, \qquad \omega = 2\pi f^* l_\infty / U_\infty^* \tag{22}$$

The stability analysis considered here is based on the spatial theory where ω is real and α and β are complex. The real and imaginary parts of α give the wave number and the disturbance growth rate, respectively, and unstable disturbance is expected for $-\alpha_i > 0$. Details of the preceding formulation may be found in Ref. 4.

Boundary Conditions

The solution of linearized stability equations requires proper boundary conditions in the normal direction. At the wall, the homogeneous Dirichlet conditions are applied. At the shock, three types of boundary conditions can be considered: 1) homogeneous boundary conditions as $\eta \to \infty$, 2) asymptotic boundary conditions at some finite distance from the wall, and 3) shock boundary conditions based on the linearized Rankine–Hugoniot conditions.

Detailed studies on the implementation of shock boundary conditions into the classical local stability analysis have been conducted for a Mach 8 flow over a 5-deg wedge (similarity solution).[4,23,24] The effect of various boundary conditions has been found to be small, except at very small wave numbers. In the region of significant amplification, the growth rates of both oblique first modes and two-dimensional second modes are unaffected by the choice of the outer boundary conditions. Similar results have been obtained for the flow over the blunt cone.

Numerical Stability Analysis

The stability equations are solved using both spectral and fourth-order Euler–Maclaurin compact methods for prototype flows to validate the stability codes (see Ref. 4). These methods provide for analysis of temporal or spatial growth. The spatial stability codes were partially verified by setting all of the curvature terms equal to zero and then solved for flow over an adiabatic flat plate with the edge conditions of $M_e = 4.5$ and $Re_{e,l} = 1.5 \times 10^3$, with $\omega = 0.23$ and $\beta = 0$. For this case, excellent agreement was found[4,5] with Malik's computation.[25]

Basic Flow Results

To verify the accuracy of the basic flow obtained by solving the PNS equations, the present computations are compared with the results of the TLNS model and experimental data for the STDS blunt-cone case. For comparison, the inviscid flow has also been analyzed over a 7-deg sharp cone at Mach 8 by solving the Taylor–Maccoll equations with a fourth-order Runge–Kutta method. The shock angle, surface pressure, and surface Mach number are obtained as $\delta_s = 10.2965$ deg, $p_e^*/p_\infty^* = 2.6025$, and $M_e = 6.8369$, respectively.

For the STDS blunt-cone case, a sensitivity study of the basic state solutions (including profiles and their derivatives) obtained by the PNS and IPNS models is investigated. The effect of grid size in the wall-normal direction and amount of numerical dissipation used in the PNS equations is also studied. All profiles and their derivatives calculated by the PNS, IPNS, and TLNS models are presented at the marching station, $S^*/R_N = 175$.

Sensitivity Study of Basic State Solutions

A grid independence study is conducted to evaluate the effects of grid size on the basic state variables. Figure 3 presents the effect of grid refinement on the Mach number profile for the STDS blunt-cone case computed by the PNS model at station 175. The results of the PNS model are presented for various number of grid points in the wall-normal direction (Jmax) with the stretching parameter equal to $\bar{\beta} = 1.01$. The numerical results suggest that Jmax $= 200$ with $\bar{\beta} = 1.01$ are sufficient for the computation of the flowfield. The dotted line in Fig. 3 shows the extent of the subsonic region.

Figure 4 shows the computed shock shape obtained by the PNS solution, which compares very well with the STDS blunt-cone experiment and the TLNS solution. Comparison of the surface pressure obtained from the PNS solution, the TLNS solution, and the inviscid sharp cone with the STDS blunt-cone experiment is made in Fig. 5. The computed results of the PNS model exhibit good agreement with those of the TLNS model and experiment. The blunt-cone surface pressure is higher than that of the inviscid sharp cone because of the displacement effect of the boundary layer. The pressure initially overexpands with respect to the asymptotic afterbody pressure and very slowly approaches the pressure of the conical flow from below.

Figure 6 presents the effect of numerical dissipation value in the PNS solution on the surface temperature distribution. Figure 6 demonstrates that the increase of the dissipation value causes a decrease of the surface temperature. With the decreasing value of numerical dissipation, the surface temperature computed by the PNS model converges to the solution of the TLNS model. Therefore, the numerical implementation of the PNS equations, for an accurate computation of the basic state variables, should use a numerical dissipation that is as small as possible. The maximum discrepancy between the computed and measured wall temperatures is about 15% (not shown in Fig. 6). It appears that the adiabatic wall condition is not a very good approximation of the experimental wall condition.

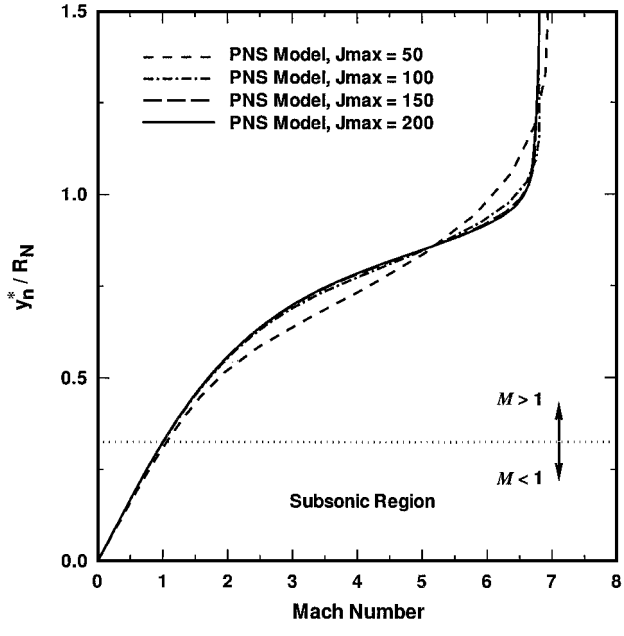

Fig. 3 Effect of grid refinement on Mach number profile in the PNS solution for the STDS blunt-cone case; $M_\infty = 8$ and $Re_\infty = 3.125 \times 10^4$ at $S^*/R_N = 175$.

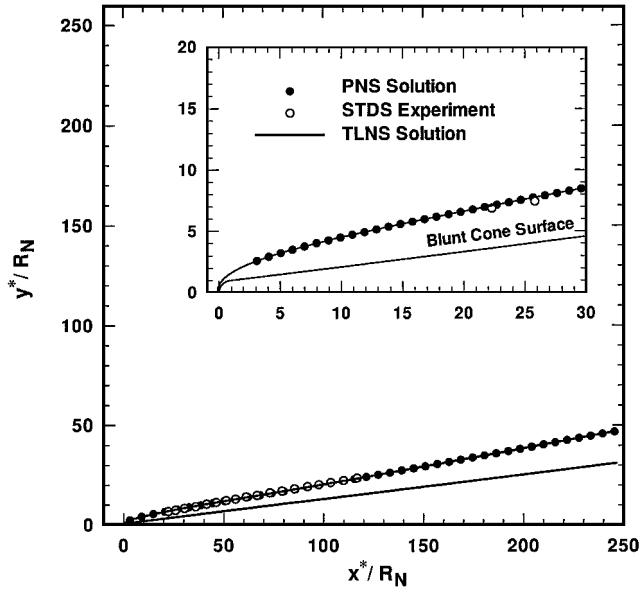

Fig. 4 Comparison of shock shape for the STDS blunt-cone case; $M_\infty = 8$ and $Re_\infty = 3.125 \times 10^4$.

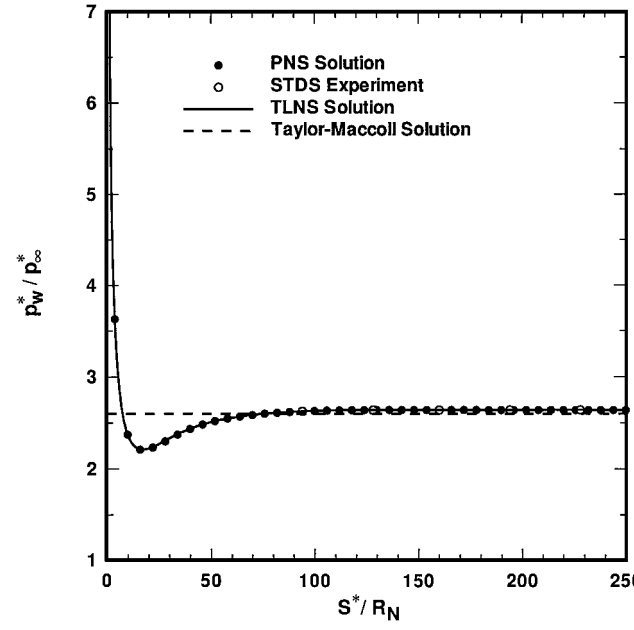

Fig. 5 Comparison of surface pressure distribution for the STDS blunt-cone case; $M_\infty = 8$ and $Re_\infty = 3.125 \times 10^4$.

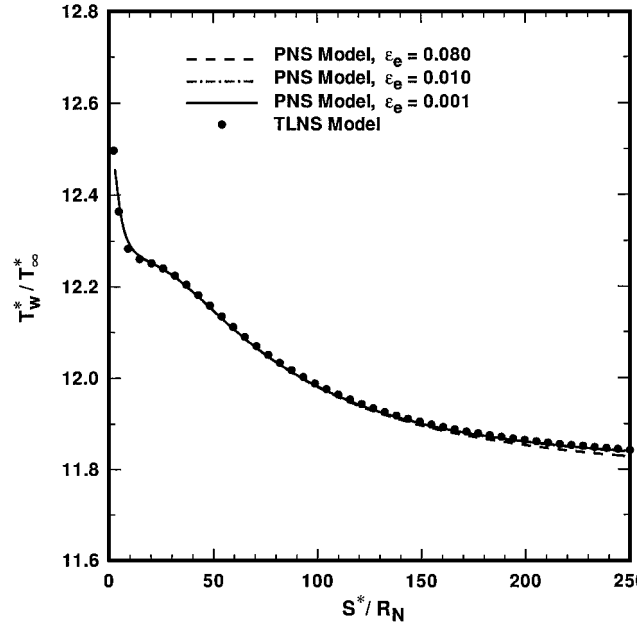

Fig. 6 Effect of numerical dissipation value on surface temperature distribution in the PNS solution for the STDS blunt-cone case; $M_\infty = 8$ and $Re_\infty = 3.125 \times 10^4$.

The IPNS model is used to improve the accuracy of the basic flow characteristics for the STDS blunt-cone case. The IPNS model is started from the upstream location of the inflection point of pressure where the pressure decreases vs streamwise position until an arbitrary downstream location (Fig. 5). For the STDS blunt-cone case, the computations are considered to be converged when the root mean square of the relative change in pressure is less than 1.0×10^{-6}. The calculations are performed for the global region $3 \leq S^*/R_N \leq 315$ for two values of $\Delta t/\Delta\xi = 1.0$ and 5.0. For $\Delta t/\Delta\xi = 1.0$, with no underrelaxation $\Omega_p = 1.0$, the number of streamwise sweeps required for convergence of the solution is about 46, and further reducing the underrelaxation term to $\Omega_p = 0.7$ does not improve the convergence rate. For $\Delta t/\Delta\xi = 5.0$, the use of the underrelaxation term substantially reduces the number of iterations. In this case, with the underrelaxation term $\Omega_p = 0.7$, the number of streamwise sweeps for convergence is about 15. For the STDS blunt-cone case, the results of the basic flowfield computed by the IPNS model are in closer agreement with the TLNS model than the PNS model, as shown in the following paragraphs.

For the stability computations, the following derivatives are required from the basic flow:

$$\frac{\mathrm{d}U}{\mathrm{d}y_n}, \quad \frac{\mathrm{d}^2U}{\mathrm{d}y_n^2}, \quad \frac{\mathrm{d}T}{\mathrm{d}y_n}, \quad \frac{\mathrm{d}^2T}{\mathrm{d}y_n^2}, \quad \frac{\mathrm{d}p}{\mathrm{d}y_n}, \quad \cdots \quad (23)$$

where y_n is the coordinate normal to the wall. These derivatives, which are obtained from the numerical solutions of the TLNS, PNS, and IPNS models, are compared with each other to examine the accuracy of the PNS and IPNS solutions. In the present study, the second-order finite difference formula is used to compute the derivatives. Note that the value of σ in Eq. (3) is set close to one to avoid oscillations in the higher derivatives of the basic flow profiles computed by the PNS model near sonic line.

Figure 7 shows a comparison of the first derivative of velocity profile DU for the three models at station 175. A small deviation exists in the first derivative of velocity profile for the PNS model near the wall, but results of the IPNS and TLNS models agree very well. In the subsonic region, the PNS model has a shear stress higher than those computed by the IPNS and TLNS models. The maximum deviation of the PNS and other solutions is at the wall. This deviation decreases as the wall-normal distance increases such that all of the solutions have approximately the same results at the sonic layer. For a single-sweep PNS model, only a fraction of the streamwise pressure gradient term $[\bar{\omega}(\partial p/\partial\xi)]$ can be retained in the subsonic region in which this term approaches zero at the wall. Because the case under study has an adverse pressure gradient, neglecting the explicit part of the streamwise pressure gradient term causes the flow to accelerate, and therefore, the velocity profile of the PNS model has a slope higher than those of the IPNS and TLNS models. This is not the case for the IPNS model because the IPNS model uses the full pressure gradient in the subsonic region and, therefore, gives the same results in comparison with those of the TLNS model.

Figure 8 gives a comparison of the first derivative of pressure profile Dp for the three models at station 175. The results of the PNS model for the first derivative of pressure profile agree very well with the IPNS and TLNS models, and no wiggles can be seen in the PNS and IPNS solutions. Figure 9 shows a comparison of the second derivative of temperature profile D^2T for the three models at the same station. The results of the IPNS and TLNS models are comparable, but deviations exist near the wall between the PNS model results and those of the IPNS and TLNS models. These deviations are due to dropping the elliptic part of the streamwise pressure gradient term in the subsonic region, which is not the case for the IPNS model. It can be seen that small wiggles (oscillations) appear in the

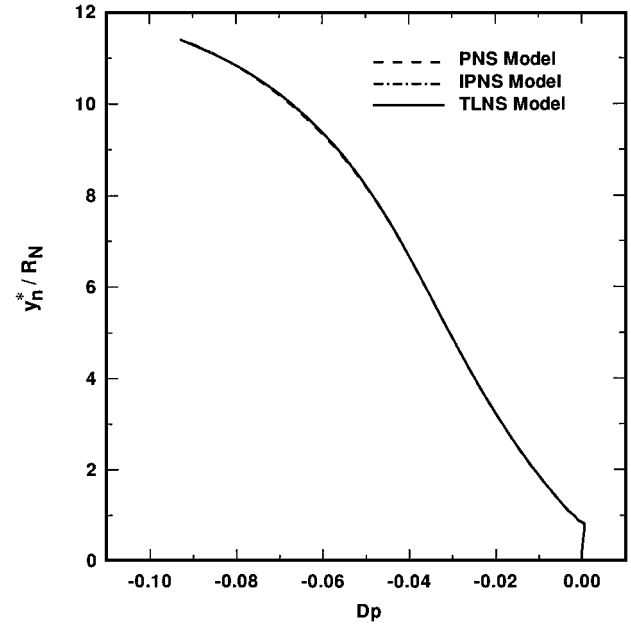

Fig. 8 Comparison of first derivative of pressure profile for the STDS blunt-cone case; $M_\infty = 8$ and $Re_\infty = 3.125 \times 10^4$ at $S^*/R_N = 175$.

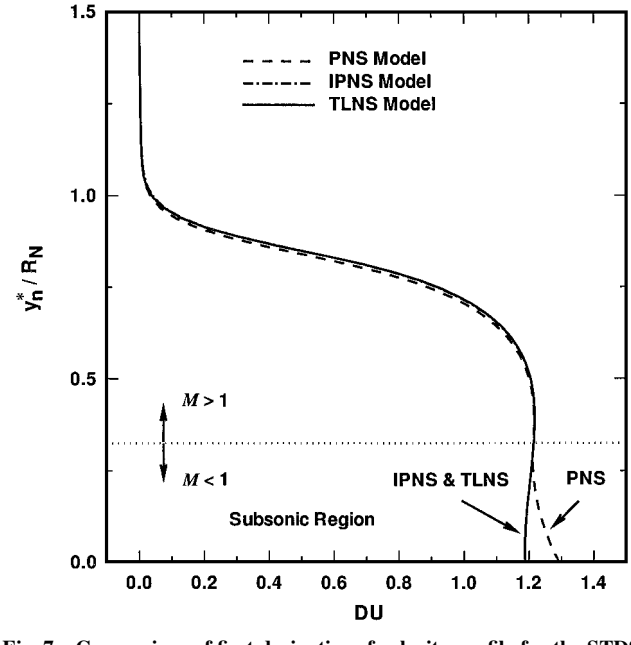

Fig. 7 Comparison of first derivative of velocity profile for the STDS blunt-cone case; $M_\infty = 8$ and $Re_\infty = 3.125 \times 10^4$ at $S^*/R_N = 175$.

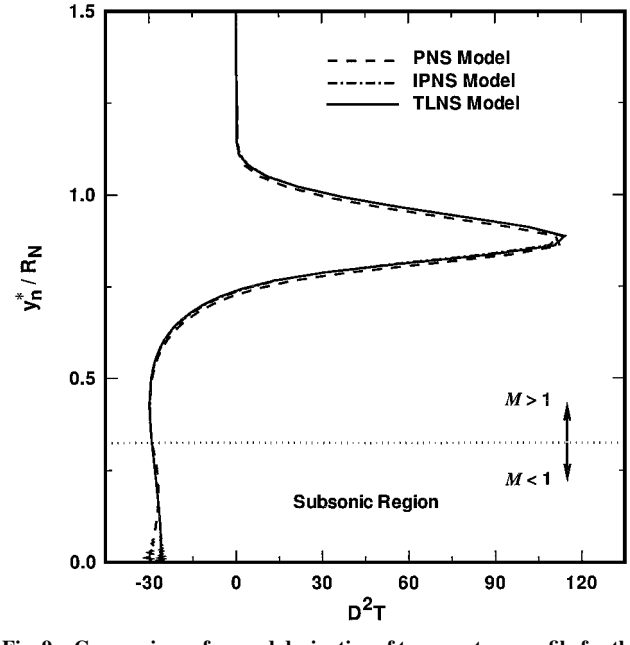

Fig. 9 Comparison of second derivative of temperature profile for the STDS blunt-cone case; $M_\infty = 8$ and $Re_\infty = 3.125 \times 10^4$ at $S^*/R_N = 175$.

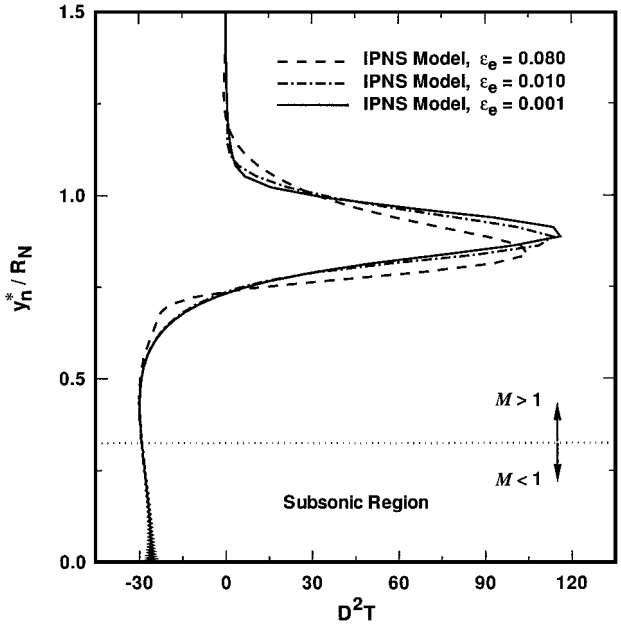

Fig. 10 Effect of numerical dissipation value on second derivative of temperature profile in the IPNS solution for the STDS blunt-cone case; $M_\infty = 8$ and $Re_\infty = 3.125 \times 10^4$ at $S^*/R_N = 175$.

D^2T profile near the wall, which may affect the stability results. These wiggles can also be seen in the results of the TLNS model. The wiggles may come from the discrete differentiation of the basic state profiles because of high clustering grid points near the wall. Note that the results of the present PNS and IPNS schemes for the basic state profiles and their first derivatives (even for pressure) show no wiggles. The results of the PNS and IPNS models show small wiggles for the higher derivatives near the wall, but the solutions are free of wiggles near the critical layer.

The effect of numerical dissipation value on the second derivative of temperature profile D^2T for the solution of IPNS model at the desired station is presented in Fig. 10. The increase of the numerical dissipation affects the value of D^2T especially near the critical layer. With decreasing the value of dissipation, this calculated profile converges to the case of the lowest dissipation value. It is also clear that for a very low dissipation value, $\epsilon_e = 0.001$, small wiggles appear in the D^2T profile near the wall. For a moderate numerical dissipation value, $\epsilon_e = 0.01$, the solutions of the PNS and IPNS models have smaller wiggles near the wall.

CPU-Time Comparison

The efficiency of the PNS and IPNS schemes is shown by the CPU-time comparison of the various solutions for the same case. Based on the TLNS model,[4] two major computations have been performed for the STDS blunt-cone case, one with (1300×100) grid points and the other with (1300×200) grid points. The total computation times on a Cray Y-MP were about 60 and 260 h, respectively. The basic flow computed by the EUBL model[7] for the STDS blunt-cone case required about 1-h CPU time on a Cray Y-MP. The present calculations are performed on a 500-MHz Pentium III computer. For the STDS blunt-cone case, based on the PNS and IPNS models (using 200 grid points in the wall-normal direction with 3120 sweeps in the streamwise direction), the maximum required memories are about 1- and 8-MB RAM, and the typical computation times are 1.5 and 20 min, respectively. The CPU time of the TLNS solution in the nose region using (40×200) grid points is about 2 h (on a personal computer), which must be added to the times of the PNS and IPNS solutions. It is clear that both the PNS and IPNS schemes significantly reduce the computer time and storage required to obtain an accurate basic flow in comparison with the TLNS model.

Stability and Transition Results

For hypersonic flows, the experiments by Stetson[1] and Stetson et al.[2] and also the prediction by Mack[26] clearly indicate the emergence of second-mode instability. It is also found that second-mode waves are most amplified when they are axisymmetric. Therefore, the stability results and the prediction of the transition location are based on the two-dimensional second-mode computations. To determine the location of the transition onset, the classical linear stability theory in conjunction with the e^N method is employed. The N factor is defined by the envelope of the total amplification curves as follows:

$$N = \max_f \left[\ln\left(\frac{A}{A^\circ}\right) \right] = \max_f \left[-\int_{\xi^\circ}^{\xi} \alpha_i \, d\xi \right] \tag{24}$$

in which $A = A(\xi)$ is the disturbance amplitude and A° refers to the streamwise position ξ°, where the disturbance becomes amplified.

Sensitivity Study of Stability Results

After the accuracy of the basic flow is examined, a sensitivity study is performed for the second-mode spatial growth rates calculated by the PNS and IPNS models. The numerical aspects affecting the stability results are identified as the number of grid points and grid distribution in the wall-normal direction and the amount of numerical dissipation used in the PNS equations.

A grid refinement study of the STDS sharp-cone case is conducted to examine the effects of number of grid points and grid distribution on the stability results. For the STDS sharp-cone case, the stability results are presented at the marching location, $S^*/S^*_{\max} = 0.326$. At this station, the local Reynolds number based on boundary-layer edge conditions is approximately $Re_{e,l} = 1.73 \times 10^3$. Figure 11 shows the spatial growth rates obtained by the PNS model for various number of grid points in the wall-normal direction, Jmax, and stretching parameter $\bar{\beta}$ at $Re_{e,l} = 1.73 \times 10^3$. The study demonstrates that the stability results are quite sensitive to the number of grid points and grid distribution used to compute the basic flow. This sensitivity is more pronounced near the branches of neutral curve. It is clear that, beyond 200 grid points, the spatial growth rate does not change very much near its peak, but it changes considerably near the neutral curve. It is also evident that a clustering parameter of 1.01 will be a better choice than 1.001 because this leads to a higher number of grid points near the critical layer. Note that the effect of stretching parameter $\bar{\beta}$ on the stability results is more pronounced for the lower number of grid points. A similar behavior was observed for the IPNS model.

For the STDS sharp-cone case, the present calculations based on the PNS and IPNS models using Jmax $= 200$ and $\bar{\beta} = 1.01$ are compared to the available theoretical results of Mack[26] and

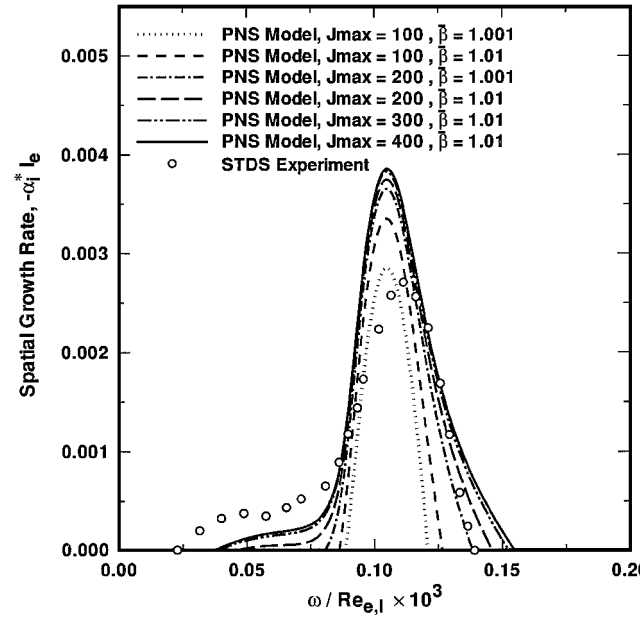

Fig. 11 Effect of grid refinement on spatial growth rates in the PNS solution for the STDS sharp-cone case; $M_\infty = 8$ and $Re_\infty = 6.525 \times 10^6$ at $Re_{e,l} = 1.73 \times 10^3$.

Chang et al.[23] at the same station, as shown in Fig. 12. It can be seen that the stability results computed by Chang et al. are comparable with the present solutions near the neutral branches, but the maximum spatial growth rate is lower than those obtained by the PNS and IPNS models.

The results of the present study (both PNS and IPNS) for the STDS sharp-cone case are nearly the same as Mack's results.[26] The differences between the present computations and Mack's results are caused by both different basic flows and different stability codes. Mack used locally planar flow and neglected all $1/h_3$ terms (curvature terms). He computed the basic flow using the boundary-layer equations with edge boundary conditions specified as the inviscid solution at the cone surface ($M_e = 6.8$ for this case). This approach ignores the inviscid–viscous interaction. Figure 13 shows a comparison of the second-mode spatial growth rates obtained by the present stability analysis with those of the planar stability study by Mack. To

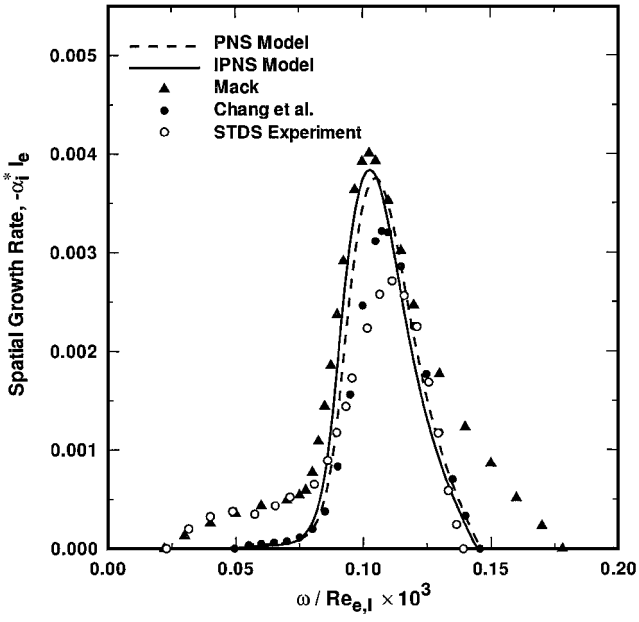

Fig. 12 Comparison of computed and measured spatial growth rates for the STDS sharp-cone case; $M_\infty = 8$ and $Re_\infty = 6.525 \times 10^6$ at $Re_{e,l} = 1.73 \times 10^3$.

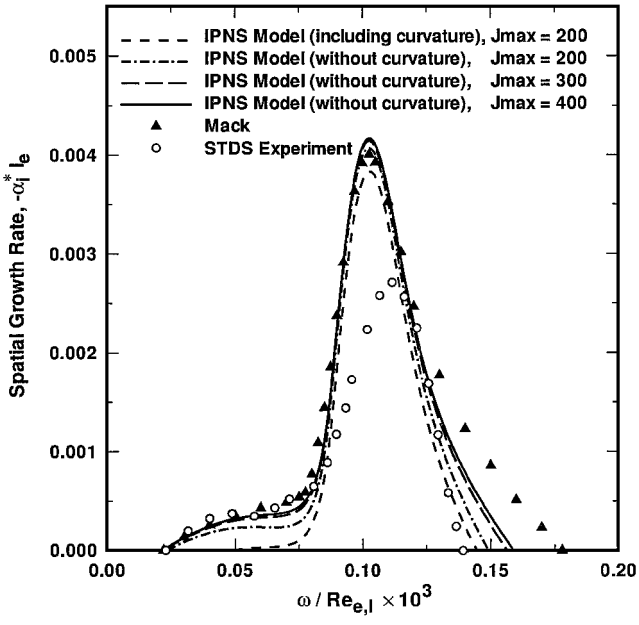

Fig. 13 Effect of curvature terms on spatial growth rates in the IPNS solution for the STDS sharp-cone case; $M_\infty = 8$ and $Re_\infty = 6.525 \times 10^6$ at $Re_{e,l} = 1.73 \times 10^3$.

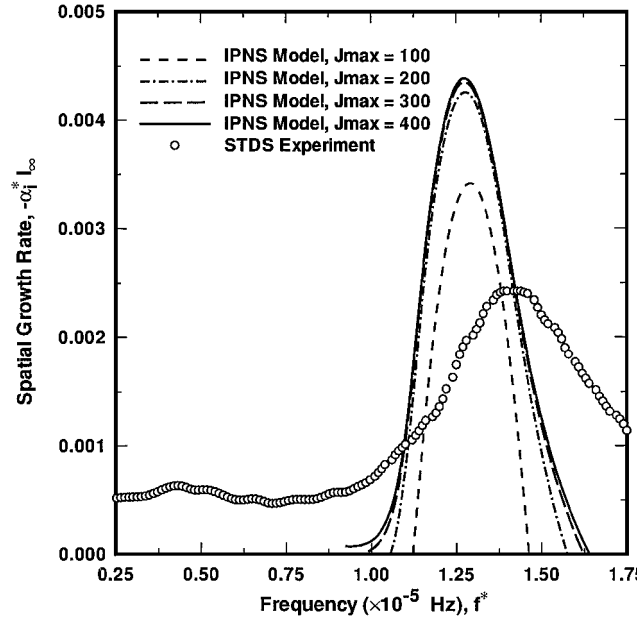

Fig. 14 Effect of grid refinement on spatial growth rates in the IPNS solution for the STDS blunt-cone case; $M_\infty = 8$ and $Re_\infty = 3.125 \times 10^4$ at $S^*/R_N = 175$.

explain the discrepancy, the present results based on the IPNS model are reproduced without curvature terms in the stability analysis. It is found that the second-mode spatial growth rates using the present study with curvature terms are always lower than the planar stability results. In fact, curvature terms in the stability analysis have a damping effect on the second-mode spatial growth rates.[27] It can be seen that the present stability results without curvature terms are in good agreement with Mack's results[26] except for the right branch of second mode. The differences in the stability results of Mack and the present study (without curvature terms) are caused by the inviscid–viscous interaction, which was neglected in Mack's computation. A similar effect was observed by Stilla[7] for the STDS blunt-cone case when the inviscid–viscous interaction was not considered in his study. The results of the IPNS model without curvature terms using 300 and 400 grid points with $\bar{\beta} = 1.01$ are also presented in Fig. 13 to show the sensitivity of the stability results to the mesh refinement.

A grid refinement study of the spatial growth rates obtained by the IPNS model for the STDS blunt-cone case at $S^*/R_N = 175$ is also performed, as shown in Fig. 14. Note that the number of grid points required for stability analysis is much larger than that used in the basic flow computations. The upper bound of number of grid points required for an accurate solution of stability can be found from the convergence of the generalized inflection profile G shown in Fig. 15. As shown in Fig. 15, the G profile converges after 200 grid points except near its peak. It takes 400 grid points or more for full convergence of the G profile. The problem is that increasing the number of grid points from 200 to 400 only adds a few grid points near the high gradient region of the G profile. This is because of the conflicting requirement of grid distribution between the basic flow and stability computations. However, as in the case of STDS sharp cone, the stability results indicate that 200 grid points with $\bar{\beta} = 1.01$ give a reasonable solution, and for even better accuracy, a higher number of grid points can be used. For the STDS blunt-cone case, with Jmax $= 300$ (or more) and $\bar{\beta} = 1.01$, the solutions of the PNS and IPNS models using the step size $\Delta\xi = 0.1$ are numerically unstable at the shock boundary. Therefore, for the results presented in Figs. 14 and 15, the step size in the marching direction is reduced by half ($\Delta\xi = 0.05$) to provide stable marching near the shock.

A mesh refinement study is also performed in the streamwise direction for both the STDS blunt and sharp cones (not presented here). It is also found that, for 200 grid points in the crossflow direction, the stability results are not very sensitive to the step size in the marching direction. The stability results based on the TLNS

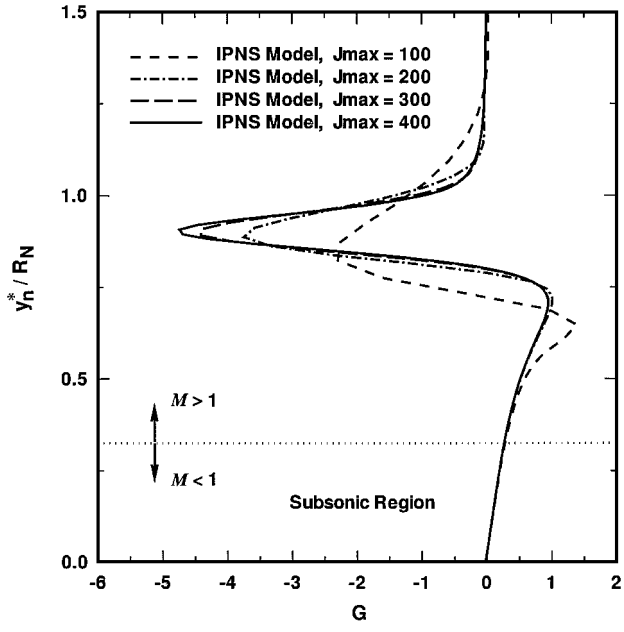

Fig. 15 Effect of grid refinement study on generalized inflection profile in the IPNS solution for the STDS blunt-cone case; $M_\infty = 8$ and $Re_\infty = 3.125 \times 10^4$ at $S^*/R_N = 175$.

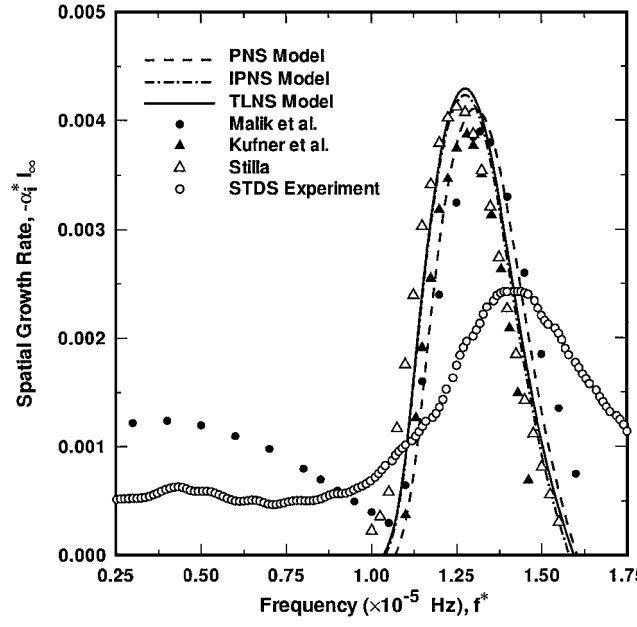

Fig. 17 Comparison of computed and measured spatial growth rates for the STDS blunt-cone case; $M_\infty = 8$ and $Re_\infty = 3.125 \times 10^4$ at $S^*/R_N = 175$.

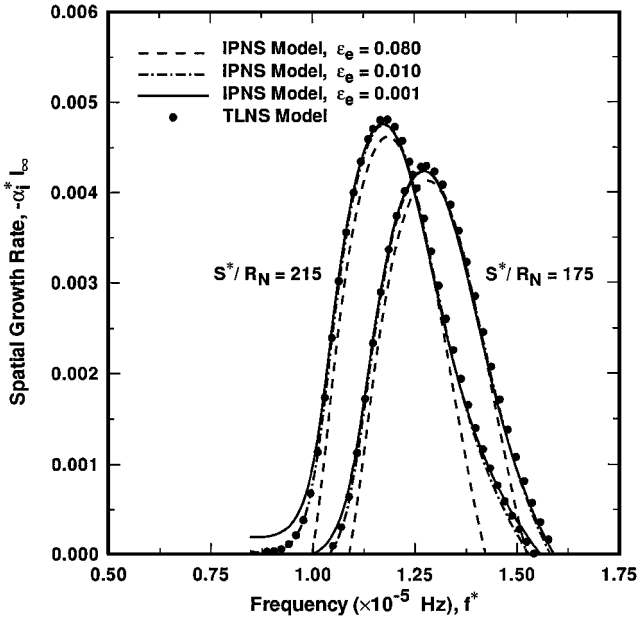

Fig. 16 Effect of numerical dissipation value on spatial growth rates in the IPNS solution for the STDS blunt-cone case; $M_\infty = 8$ and $Re_\infty = 3.125 \times 10^4$ at $S^*/R_N = 175$ and 215.

model for the STDS blunt-cone case are available for Jmax $= 200$ and $\bar{\beta} = 1.01$. Hence, for all of the following comparisons on the STDS blunt-cone case, the results of the PNS and IPNS models are presented with Jmax $= 200$ and $\bar{\beta} = 1.01$ using $\Delta\xi = 0.1$.

The effect of numerical dissipation value in the IPNS solution on the spatial growth rates at two different stations is investigated for the STDS blunt-cone case, as shown in Fig. 16. It can be seen that the increase of the numerical dissipation value lowers (damps) the second-mode curve and decreases the maximum growth rate, and the bandwidth of instability becomes much narrower. Consequently, the stability results change especially near the neutral curve, which may affect the location of transition. This behavior is more pronounced at the farther streamwise location. It seems that the shift of growth rate curve from the left to the right side is due to the increase of the numerical dissipation value in computing the basic flow using the IPNS model. A similar behavior was observed for the PNS model. As mentioned before, the small wiggles appear in higher derivatives in the subsonic region for a very low dissipation value. However, the present stability computations show that the wiggles in the higher derivatives near the wall produced by the PNS and IPNS solutions do not affect the stability results very much for hypersonic flow because the critical layer is near the edge of boundary layer. This study indicates that the choice of the numerical dissipation value equal to $\epsilon_e = 0.01$ gives reasonable results for the stability in comparison with the results of the TLNS model.

The results for the second-mode spatial growth rates vs frequency at station 175 are shown in Fig. 17 for the PNS, IPNS, and TLNS models together with those of Malik et al.,[3] Kufner et al.,[6] Stilla,[7] and the STDS blunt-cone experiment.[2] At this station, the local Reynolds number based on the PNS and IPNS solutions is $Re_{\infty,l} = 2.33853 \times 10^3$, the same as the TLNS result. The wave number $\alpha_r = 0.21$ at the frequency of maximum amplification corresponds to a wavelength twice that of the boundary-layer thickness, as observed by the STDS blunt-cone experiment. The maximum growth rate, however, is significantly different from the observed value, and the bandwidth of instability is much narrower, similar to that observed in the STDS sharp-cone experiment. The stability results obtained from the PNS and IPNS models are qualitatively in good agreement with those based on the other basic flow models. Stilla[7] showed that the differences between his and Esfahanian's stability results[4] are due to different basic flows and not due to different stability codes. Similar conclusions can be made about stability results based on the PNS and IPNS models as basic flows in comparison with Stilla's results[7] based on the EUBL model. Although the results of the IPNS model are closer to the results of the EUBL model than those of other models, it is not clear why such differences between the IPNS and EUBL models should exist. According to Fig. 17, the results of the PNS model are closer to the TLNS results than those of Malik et al.[3] and Kufner et al.,[6] whereas the IPNS and TLNS results are almost identical. It can be seen that the IPNS model shifts the maximum growth rate to a larger value and moves the whole curve to the left side, which is closer to the results of the TLNS model than those of the PNS model. A similar effect can be seen for the STDS sharp-cone case (Fig. 12).

As shown in Fig. 17, the maximum spatial growth rates obtained by Malik et al.[3] and Kufner et al.[6] are lower than those of computed by the PNS, IPNS and TLNS models. The numerical methods used by Malik et al.[3] and Kufner et al.[6] to compute the basic flow are different than the one used here. In fact, different numerical methods mean different numerical dissipations that result in different stability

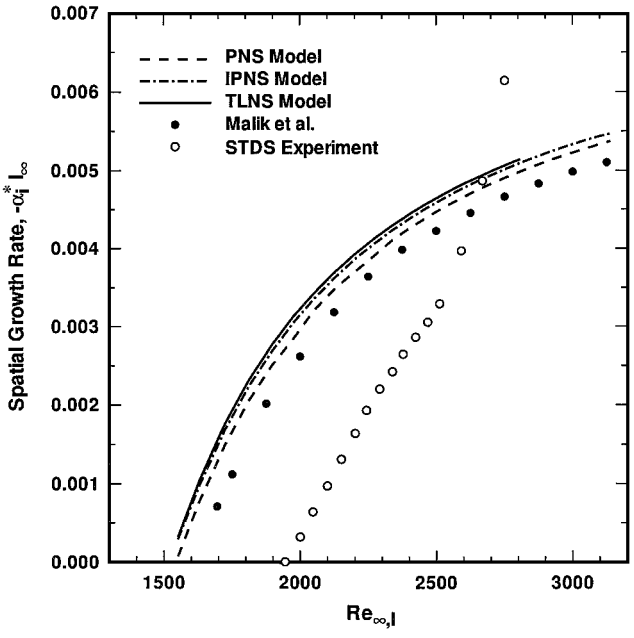

Fig. 18 Comparison of computed and measured maximum spatial growth rates for the STDS blunt-cone case; $M_\infty = 8$ and $Re_\infty = 3.125 \times 10^4$.

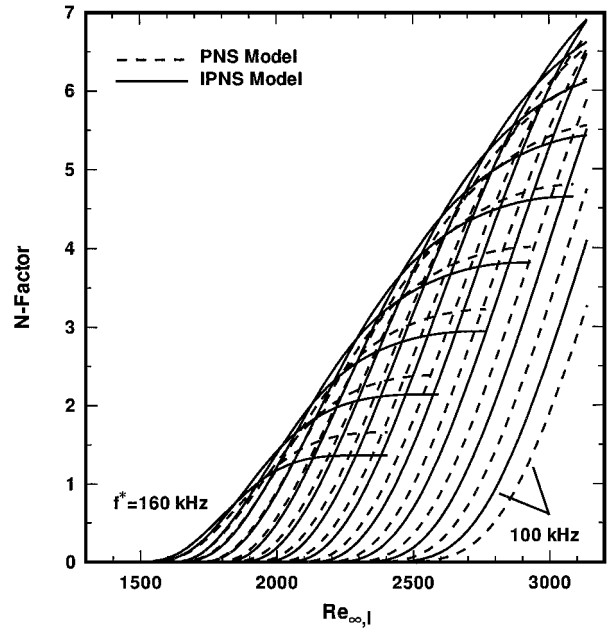

Fig. 19 Second-mode N-factor computation for the STDS blunt-cone case; $M_\infty = 8$ and $Re_\infty = 3.125 \times 10^4$ ($\Delta f^* = 5$ kHz).

results. The present sensitivity study demonstrates that the number of grid points, the grid distribution, and also the numerical dissipation can affect the stability results. Therefore, their underpredictions might be due to unsuitable grid size and grid distribution or due to inherent numerical dissipation that may exist in their numerical methods of basic flow solutions. Similar discussion applies to the STDS sharp-cone case in which the PNS code used by Chang et al.[23] underpredicts the maximum spatial growth rate in comparison with the present stability results.

For the STDS blunt and sharp cones, the stability results based on the PNS and IPNS models show much larger maxima for the second-mode spatial growth rates than the experimental results. The main reason for the discrepancy between the experimental results and the present computations seems to be the presence of wind-tunnel noise. According to Wilkinson,[28] linear stability theory is capable of predicting a large portion of the instability process only when the relevant physics are included and the experimental data are obtained in a suitably low-disturbance environment, which may not be the case in the STDS experiments. Note that the stability results of the sharp-cone case show a better agreement with the experimental data than those of the blunt-cone case. This may be due to the presence of the entropy layer for the blunt cone.

Figure 18 compares the computed maximum growth rates vs local Reynolds number $Re_{\infty,l}$ from the PNS, IPNS, and TLNS models with the results of Malik et al.[3] and the STDS blunt-cone experiment. Note that the stability results based on the PNS and IPNS models are closer to the results of the TLNS model than those of Malik et al. The computed critical Reynolds number based on the PNS model (about $Re_{\infty,l} = 1.54 \times 10^3$) is qualitatively comparable with the results of the IPNS and TLNS models and that of Malik et al. All of the predicted critical Reynolds numbers are lower than the measured one ($Re_{\infty,l} = 1.95 \times 10^3$). These deviations exist up to about $Re_{\infty,l} = 2.5 \times 10^3$, and the experimental growth rate suddenly begins to increase about this Reynolds number and crosses the computed growth rate curves. The rapid change of the experiment growth rate may be due to the nonlinear effects, which can not be predicted by the linear stability theory.

Prediction of Transition Onset

Figure 19 shows the second-mode N-factor computation of the STDS blunt-cone case based on the PNS and IPNS models. For $N = 5.5$, the transition location computed by Malik et al.[3] for a sharp-cone case with the same freestream conditions was in agreement with the experimental data of Stetson et al.[14] Because the blunt-cone experiments were performed in a similar disturbance environment, $N = 5.5$ was also assumed for this case. When the same N factor, based on the PNS and IPNS models, is used, transition takes place at $Re_{\infty,l} = 2.865 \times 10^3$ ($Re_{e,S} = 11.6 \times 10^6$) and $Re_{\infty,l} = 2.825 \times 10^3$ ($Re_{e,S} = 11.3 \times 10^6$), respectively, which is comparable with the prediction by Malik et al.[3] and Stilla,[7] $Re_{\infty,l} = 2.8 \times 10^3$ ($Re_{e,S} = 11 \times 10^6$). The frequency range around the predicted transition Reynolds numbers is between 120 and 130 kHz. The computed transition Reynolds number based on the IPNS model differs from the estimate of the STDS experiment ($Re_{e,S} = 13 \times 10^6$) by only about 13%. The transition location predicted by the PNS model is expected to be higher than that of the IPNS model for the STDS blunt-cone case. This is due to omitting part of unfavorable streamwise pressure gradient term in the PNS model, which delays the transition location.

Conclusions

The accuracy of the PNS and IPNS models for use as basic flows for stability analysis of hypersonic laminar flow over blunt and sharp cones at Mach 8 has been studied. Some conclusions regarding the basic state and stability computations of hypersonic flow over slender axisymmetric bodies are as follows:

1) The basic flowfield computed by the PNS model is in good agreement with the TLNS model and experimental data. The results of the IPNS model indicate that the global iteration of the PNS solution improves the accuracy of basic flow variables and their derivatives. The PNS and IPNS models significantly reduce the computation time and memory needed to obtain an accurate basic flow in comparison with the TLNS model.

2) The present results indicate that the accuracy of basic flow variables and their derivatives computed by the PNS equations is sensitive to the amount of numerical dissipation. The sensitivity study shows that the most sensitive variable, which is affected by the numerical dissipation, is temperature. The study demonstrates that the increase of the numerical dissipation value affects the higher derivatives of the basic state profiles especially near the critical layer. Therefore, the numerical implementation of the PNS and IPNS models should use as small as possible numerical dissipation value.

3) The sensitivity study shows that the number of grid points and the grid distribution have significant effects on the stability results. The study indicates that an accurate solution requires a sufficiently fine grid close to the wall, especially near the critical layer. The generalized inflection profile G is a good indicator for the upper bound of number of grid points required for accurate stability computations.

4) The stability characteristics such as the spatial growth rates, the critical Reynolds number, and the transition location predicted by the PNS model qualitatively agree with those based on other basic flow models. The present study shows that the stability results are almost identical for both IPNS and TLNS as a basic flow.

5) The present study indicates that the wiggles in higher derivatives near the wall produced by the PNS and IPNS solutions do not affect the stability and transition results very much for hypersonic flow, where the critical layer is near the edge of the boundary layer.

6) It is found that the increase of the numerical dissipation value lowers (damps) the second-mode spatial growth rate curve and decreases the maximum growth rate, and the bandwidth of instability becomes much narrower, especially near the neutral curve. In fact, the numerical dissipation has a stabilizing influence on the second-mode spatial growth rate. However, the effect of numerical dissipation on the stability results is not as great as those of number of grid points and grid distribution. An additional effect of increase of numerical dissipation value on the stability results is to shift the second-mode growth rate curve from the left to the right side.

7) The present study demonstrates the suitability of using more computationally efficient parabolized schemes for stability calculations in comparison with Navier–Stokes and Euler/boundary-layer solutions and shows that the PNS schemes produce nearly the same results. The study indicates that careful numerical solutions of the PNS and IPNS models can be used for a rapid and practical transition prediction in hypersonic flow over axisymmetric geometries.

Acknowledgments

The authors would like to thank the University of Tehran for financial support of this project. The authors also wish to acknowledge the reviewers for their helpful suggestions, which have been incorporated in the final manuscript.

References

[1]Stetson, K. F., "Effect of Bluntness and Angle of Attack on Boundary-Layer Transition on Cone and Biconic Configuration," AIAA Paper 79-0269, Jan. 1979.

[2]Stetson, K. F., Thompson, E. R., Donaldson, J. C., and Siler, L. G., "Laminar Boundary Layer Stability Experiments on a Cone at Mach 8, Part 2: Blunt Cone," AIAA Paper 84-0006, Jan. 1984.

[3]Malik, M. R., Spall, R. E., and Chang, C. L., "Effect of Nose Bluntness on Boundary Layer Stability and Transition," AIAA Paper 90-0112, Jan. 1990.

[4]Esfahanian, V., "Computation and Stability Analysis of Laminar Flow over a Blunted Cone in Hypersonic Flow," Ph.D. Dissertation, Dept. of Aeronautical and Astronautical Engineering, The Ohio State Univ., Columbus, OH, June 1991.

[5]Herbert, T., and Esfahanian, V., "Stability of Hypersonic Flow over a Blunt Body," CP-514, AGARD, May 1992.

[6]Kufner, E., Dallmann, U., and Stilla, J., "Instability of Hypersonic Flow past Blunt Cones-Effects of Mean Flow Variations," AIAA Paper 93-2983, July 1993.

[7]Stilla, J., "Engineering Transition Prediction for a Hypersonic Axisymmetric Boundary Layer," *Journal of Aircraft*, Vol. 31, No. 6, 1994, pp. 1358–1364.

[8]Beam, R. M., and Warming R. F., "An Implicit Factored Scheme for the Compressible Navier–Stokes Equation," *AIAA Journal*, Vol. 16, No. 4, 1978, pp. 393–402.

[9]Esfahanian, V., and Hejranfar, K., "Numerical Simulation of Axisymmetric Steady Supersonic Laminar Viscous Flow Using PNS Equations," *Journal of Faculty of Engineering, University of Tehran*, Vol. 31, No. 1, 1998, pp. 83–100.

[10]Esfahanian, V., and Hejranfar, K., "The Use of Global Procedure of the PNS Equations for Solving Supersonic Flows with Upstream Influences," *First International Conference of the Iranian Aerospace Society*, Vol. 1, Jan. 2000, pp. 279–290.

[11]Esfahanian, V., Herbert, T., and Burggraf, O. R., "Computation of Laminar Flow over a Long Slender Axisymmetric Blunted Cone in Hypersonic Flow," AIAA Paper 92-0756, Jan. 1992.

[12]Esfahanian, V., and Hejranfar, K., "The Accuracy of PNS Equations as a Basic Flow for Stability Analysis of Laminar Flow over a Blunt Cone," *Sixth Annual Conference of the Computational Fluid Dynamics Society of Canada*, Computational Fluid Dynamics Society of Canada, Quebec, QC, Canada, 1998, Pt. 8, pp. 37–44.

[13]Esfahanian, V., and Hejranfar, K., "Computation and Transition Prediction of Hypersonic Axisymmetric Flow Using IPNS Model," *European Congress on Computational Methods in Applied Sciences and Engineering*, Barcelona, 2000, pp. 1–17.

[14]Stetson, K. F., Thompson, E. R., Donaldson, J. C., and Siler, L. G., "Laminar Boundary Layer Stability Experiments on a Cone at Mach 8, Part 1: Sharp Cone," AIAA Paper 83-1761, July 1983.

[15]Hsieh T., "Heat Transfer Calculation for Hypersonic Flow over a Spherical Blunt Noses Using an Unsteady Implicit Scheme," *Proceedings of the Second National Symposium on the Numerical Methods in Heat Transfer*, Hemisphere, Washington, DC, 1982, pp. 375–401.

[16]Tannehill, J. C., Anderson, D. A., and Pletcher, R. H., *Computational Fluid Mechanics and Heat Transfer*, 2nd ed., Taylor and Francis, Washington, DC, 1997.

[17]Vigneron, Y. C., Rakich, J. V., and Tannehill, J. C., "Calculation of Supersonic Viscous Flow over Delta Wings with Sharp Subsonic Leading Edges," AIAA Paper 78-1137, July 1978.

[18]Schiff, L. B., and Steger, J. L., "Numerical Simulation of Steady Supersonic Viscous Flow," *AIAA Journal*, Vol. 18, No. 12, 1980, pp. 1421–1430.

[19]Rubin, S. G., "A Review of Marching Procedures for Parabolized Navier–Stokes Equations," *Proceedings of Symposium on Numerical and Physical Aspects of Aerodynamic Flows*, Springer-Verlag, New York, 1982, pp. 171–185.

[20]Rakich, J. V., "Iterative PNS Method for Attached Flows with Upstream Influence," AIAA Paper 83-1955, July 1983.

[21]Barnett, M., and Davis, R. T., "Calculation of Supersonic Flows with Strong Viscous–Inviscid Interaction," *AIAA Journal*, Vol. 24, No. 12, 1986, pp. 1949–1455.

[22]Cline, D. D., and Carey, G. F., "Conflicting Stepsize Requirements for Stable PNS Computations," AIAA Paper 89-0445, 1989.

[23]Chang, C. L., Malik, M. R., and Hussaini, M. Y., "Effects of Shock on the Stability of Hypersonic Boundary Layers," AIAA Paper 90-1448, June 1990.

[24]Esfahanian, V., "The Effect of a Shock on Flow Stability Using a Model Flow," *Proceedings of the 1996 Engineering System Design and Analysis Conference*, Vol. 6, Computational Mechanics and Thermomechanics, American Society of Mechanical Engineers, Montpellier, France, 1996, pp. 129–136.

[25]Malik, M. R., "Numerical Methods for Hypersonic Boundary Layer Stability," *Journal of Computational Physics*, Vol. 86, No. 2, 1990, pp. 376–413.

[26]Mack, L. M., "Stability of Axisymmetric Boundary Layers on Sharp Cones at Hypersonic Mach Numbers," AIAA Paper 87-1413, June 1987.

[27]Malik, M. R., and Spall, R. E., "On the Stability of Compressible Flow past Axisymmetric Bodies," *Journal of Fluid Mechanics*, Vol. 228, 1991, pp. 443–463.

[28]Wilkinson, S. P., "A Review of Hypersonic Boundary Layer Stability Experiments in a Quiet Mach 6 Wind Tunnel," AIAA Paper 97-1819, June–July 1997.

P. Givi
Associate Editor